New infrared nonlinear optical crystal CsGeBr$_3$: synthesis, structure and powder second-harmonic generation properties

New infrared nonlinear optical crystal CsGeBr$_3$: synthesis, structure and powder second-harmonic generation properties

L C Tang[1,4]**, J Y Huang**[1]**, C S Chang**[1,4] **, M H Lee**[2] **and L Q Liu**[3]

[1] Department of Photonics and Institute of Electro-Optical Engineering, National Chiao Tung University, Hsinchu 305, Taiwan, Republic of China
[2] Department of Physics, Tamkang University, Taipei 251, Taiwan, Republic of China
[3] College of Materials Science and Engineering, Shandong University of Science and Technology, Shandong Province, People's Republic of China

E-mail: newton4538.eo85g@nctu.edu.tw (L C Tang) and cschang@mail.nctu.edu.tw (C S Chang)

Abstract
An innovative infrared nonlinear optical crystal CsGeBr$_3$ was synthesized. *Ab initio* calculations on CsGeBr$_3$ were also carried out in order to analyse the second-order nonlinear susceptibilities. From its powder x-ray diffraction pattern, this crystal was characterized as a rhombohedral structure with an ($R3m$, No 160) space group symmetry. The reflection powder second-harmonic generation (PSHG) measurement of CGBr showed that its nonlinear optical efficiency is 1.62 times larger than that of rhombohedral CsGeCl$_3$ and is 9.63 times larger than that of KH$_2$PO$_4$ (KDP), and most important of all that CsGeBr$_3$ is phase-matchable. The rescaled $d_{\rm eff}^{(2)}$ of CGBr was about 2.45 times larger than that of rhombohedral CsGeCl$_3$, and this trend was coincident with the *ab initio* calculation results. The infrared transparent spectrum of rhombohedral CsGeBr$_3$ was extended to more than 22.5 μm. The rhombohedral CsGeBr$_3$ shows the potential in the realm of nonlinear optics and can be applied to the infrared region.

(Some figures in this article are in colour only in the electronic version)

1. Introduction

Second-order nonlinear optical (NLO) materials have played a key role in such optical fields as laser frequency conversion and optical parametric oscillation/amplification (OPO/OPA) [1, 2]. For inorganic second-order NLO materials, several crystals used in ultraviolet (UV) and visible regions have been proposed in the past two decades, such as KH$_2$PO$_4$ (KDP), KTiOPO$_4$ (KTP),

[4] Authors to whom any correspondence should be addressed.

β-BaB$_2$O$_4$ (BBO) and LiB$_3$O$_5$ (LBO). But in the infrared (IR) region the current materials, such as AgGaSe$_2$ and ZnGeP$_2$, are not good enough for applications mainly due to their low laser damage threshold, as their bandgaps were smaller than 1.5 eV. So the search for new NLO materials in the IR region became one of the most important challenges due to their potentially wide applications in such fields as laser technology and molecular spectroscopy [3].

Recently, several ternary halides were discovered to exhibit second-order NLO properties, such as ABX$_3$ (A = Cs, Rb, B = Ge, Cd, X = Cl, Br, I) [4–6]. In particular, CsGeCl$_3$ (caesium germanium chloride, CGC), which was found to posses excellent second-order NLO properties, exhibited an SHG five times larger than that of KDP. Furthermore, its damage threshold reaches 200 MW cm^{-2} [7]. Therefore, the ternary halides recently became a new category of nonlinear optical materials, which were potentially applicable from the visible to the infrared spectrum. The crystal CsGeCl$_3$ was announced to be an innovative nonlinear (NLO) IR crystal by Ewbank *et al* [6] and Gu *et al* [8, 7, 9], respectively. The electronic and linear optical properties of CsGeI$_3$ were also reported by Tang *et al* [10]. At the same time, CsCdBr$_3$ was found by Ren *et al* [11] to be noncentrosymmetric (NCS), i.e. the symmetry of inversion centre was absent. Therefore, rhombohedral CsGeBr$_3$ should be expected in nonlinear optical applications.

To apply CsGeBr$_3$ as an infrared SHG material, it should possess the following attributes: transparency in the relevant wavelengths; ability to withstand laser irradiation and chemical stability. Most importantly, the material in question must be crystallographically NCS. Mathematically it has been known for some time that only an NCS arrangement of atoms may produce a second-order NLO response [3, 12, 13].

In order to understand the properties, which were mentioned in the previous paragraph, of CsGeBr$_3$ crystal, the synthesis and powder SHG behaviour (PSHG) of CsGeBr$_3$ were estimated. The transparency was measured in the mid-infrared range. Both the experimental and calculated lattice parameters will be compared in section 2 of this paper. Through the powder measurements, an approximate value for $d_{\text{eff}}^{2\omega}$, the NLO susceptibility, was evaluated. The PSHG results of CsGeBr$_3$ are also compared with the *ab initio* calculation results in section 3.

2. Synthesis and structural properties

Rhombohedral CsGeBr$_3$ crystal could be considered as a highly distorted perovskite crystal structure, and is shown in figure 1. The reported [14–18] lattice parameters of CsGeBr$_3$ at room temperature were $a = b = c = 5.635$ Å, $\alpha = \beta = \gamma = 88.74°$ with noncentrosymmetric rhombohedral space group $R3m$ (No 160).

Rhombohedral CsGeBr$_3$ crystal was synthesized and sieved into different particle sizes in order to measure and analyse its structural and optical properties. The measured values of CGB, synthesized in this work and by using the XRD and Rietveld refinement, will also be compared with the reported and the *ab initio* calculation results in table 1. Positions of the constituents in the rhombohedral NLO crystals CsGeBr$_3$ could be easily generated.

2.1. Synthesis

The procedure of synthesis is illustrated in figure 2, which was modified from the work done by Gu *et al* [8, 7, 9]. Christensen and Tananaev *et al* [19, 20] used different synthesis methods, but their methods seemed complex and the productivity was poor. In this study, 50% H$_3$PO$_2$ (25 ml) was loaded with 43.5% HBr (25 ml) and GeO$_2$ (5.25 g) into a 500 ml beaker, and then heated to 85–90 °C. The solution was vigorously mixed for 5 h and then cooled to room
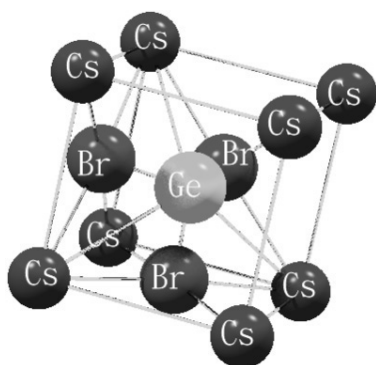
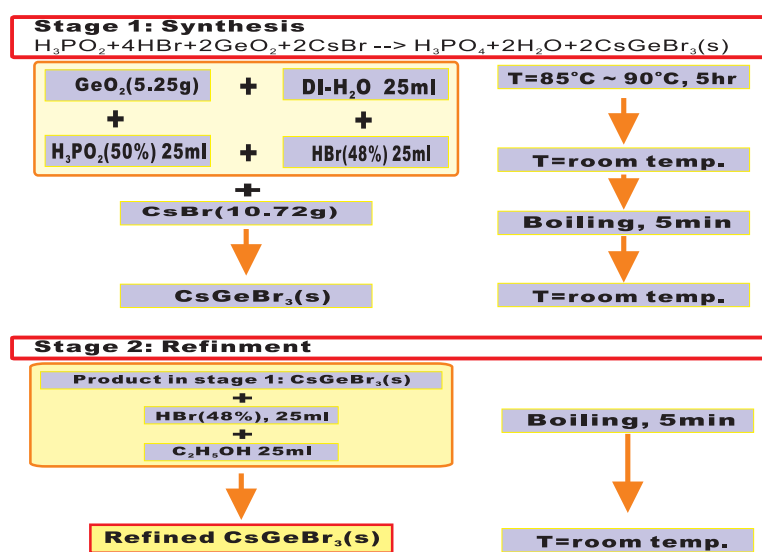**Figure 1.** The crystal structure of rhombohedral CsGeBr$_3$.

Figure 2. The synthesis procedure of rhombohedral nonlinear optical crystal CsGeBr$_3$.

Table 1. Lattice constants and the Ge's fractional coordinates of the rhombohedral NLO crystals CsGeBr$_3$ and CsGeCl$_3$. The *ab initio* calculation results and the measured values by using the XRD and Rietveld refinement were compared.

	$a(= b = c)$	$\alpha(= \beta = \gamma)$	Frac. coord. of Ge	t_G
CsGeBr$_3$ (JCPDS)	5.635(9)	88.74(4)	(0.476(4), 0.476(4), 0.476(4))	1.009(4)
CsGeBr$_3$ (exp.)	5.647(5)	88.79(3)	(0.494(1), 0.494(1), 0.494(1))	
CsGeBr$_3$ (*ab initio*)	5.688(5)	88.29(7)	(0.470(9), 0.470(9), 0.470(9))	
CsGeCl$_3$ (JCPDS)	5.434(2)	89.72(3)	(0.481(0), 0.481(0), 0.481(0))	1.027(2)
CsGeCl$_3$ (exp.)	5.446(9)	89.70(8)	(0.499(3), 0.499(3), 0.499(3))	
CsGeCl$_3$ (*ab initio*)	5.510(8)	89.12(1)	(0.479(9), 0.479(9), 0.479(9))	

temperature. After removing the precipitate, CsBr (10.72 g) was added and the temperature raised to boiling, then the mixture was naturally cooled to room temperature again. A yellow

precipitation, about 22.30 g, was formed. The reaction equations were listed as follows:

$$H_3PO_2 + 6HBr + 2GeO_2 = H_3PO_4 + 2HGeBr_3 + 2H_2O \tag{1}$$

then

$$HGeBr_3 + CsBr = CsGeBr_3\downarrow. \tag{2}$$

Recrystallization was done by mixing the precipitation $CsGeBr_3$ with 1:1 concentrated HBr and alcohol solution to give the yellow crystals $CsGeBr_3$.

2.2. X-ray diffraction

Although the structure of $CsGeBr_3$ has been reported, we felt it important to determine the structure to better understand the SHG properties. The synthesized yellow crystals $CsGeBr_3$ were crushed, ground and sieved. X-ray diffractograms were obtained at room temperature by means of Cu Kα radiation with Siemens D5000 equipment. For determination of the lattice parameters, an extra CsBr crystal was used as an internal standard. The measured pattern was indexed and analysed, i.e. the full-profile Rietveld refinement, by a non-profit program *Powder Cell* [21], which was developed by Kraus and Nolze. The structural parameters of $CsGeBr_3$, which were reported by JCPDS [14–18], are listed in table 1, for comparison.

2.3. Ab initio calculations

The *ab initio* optimized cell parameters were compared with the experimental data. The *ab initio* calculations were performed by using the plane-wave-pseudopotential approach within the framework of density-functional theory (DFT) implemented in CASTEP software [22, 23]. The summation over the Brillouin zone (BZ) was carried out with a special k-point sampling using a Monkhorst–Pack grid [24].

In order to save computation time, the special k-point set was reduced to 8 k points ($3\times3\times3$ mesh) for the calculation of the equilibrium lattice constants and mechanical properties. The equilibrium lattice constants and fractional atomic coordinates were deduced from the total-energy minimization. Relaxation of the lattice parameters and atomic positions was carried out under the constraint of the unit-cell space-group symmetry.

2.4. Discussion

There were certain stronger diffraction peaks observed at $2\theta = 31.82°, 27.68°, 22.12°, 22.62°,$ $26.86°, 45.06°$ and $46.06°$ (see figure 3). These diffraction patterns were compared with JCPDS (Joint Committee on Powder Diffraction) and *ab initio* calculated data, and were also indexed with (200), (11$\bar{1}$), (110), (1$\bar{1}$0), (111), (220) and (2$\bar{2}$0) planes, respectively. A few extra GeO_2 and CsBr were observed as references at $2\theta = 26.04°$ and $29.52°$, respectively. The cell parameters, which were refined from powder XRD, in table 1 and figure 3 confirm that $CsGeBr_3$, crystallized in the noncentrosymmetric rhombohedral space group $R3m$ with data $a = b = c = 5.647$ Å, $\alpha = \beta = \gamma = 88.79°$, compared well to the single-crystal data, $a = b = c = 5.635$ Å, $\alpha = \beta = \gamma = 88.74°$. The *ab initio* optimized cell parameters were $a = b = c = 5.688$ Å, $\alpha = \beta = \gamma = 88.29°$. The differences between calculated and measured lattice parameters were less than 0.5%, and this accurate result could almost guarantee the *ab initio* calculated SHG responses. The *ab initio* optimized cell angles of $CsGeBr_3$ and $CsGeCl_3$ were more distorted from cubic structure than the experimental ones and the reported angles were distorted. The expected *ab initio* NLO susceptibilities [25] will be larger than the experimental SHG results in $CsGeBr_3$ and $CsGeCl_3$.
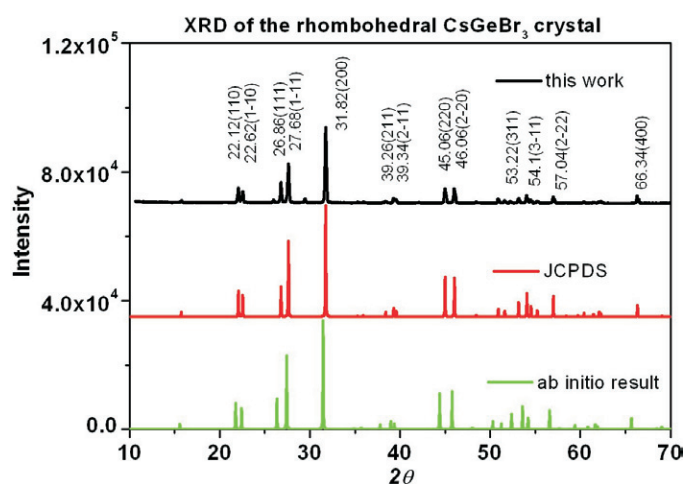
Figure 3. The data-base (JCPDS), *ab initio* estimated and measured powder x-ray diffraction pattern of rhombohedral nonlinear optical crystal CsGeBr$_3$.

In an ideal perovskite structure, the cell parameters were $a = b = c$ and $\alpha = \beta = \gamma = 90°$ with cubic space group $Pm\bar{3}m$ (No 221). Examples are the higher temperature phase of cubic CsGeCl$_3$ and CsGeBr$_3$ [14–18]. The cell parameters of cubic CsGeBr$_3$ were $a = b = c = 5.362$ Å and $\alpha = \beta = \gamma = 90°$ with space group $Pm\bar{3}m$ (No 221). The cell edges of rhombohedral (room temperature phase) CsGeBr$_3$ were longer than those of cubic (higher temperature) phase, and the cell angles of rhombohedral (room temperature phase) CsGeBr$_3$ became slightly smaller than 90°. The structural distortion was one of the contributions of CsGeBr$_3$'s optical nonlinearity. With perovskite-type ternary oxides ABO$_3$ as well as halides ABX$_3$, Goldschmidt's tolerance factor t_G [26, 27] serves as a discriminating parameter of classifying perovskites in terms of structure modifications and the resulting physical properties [28–32]. The type of stacking depends on the tolerance factor t_G [26, 27]

$$t_G = \frac{(r_A + r_X)}{\sqrt{2}(r_B + r_X)}, \tag{3}$$

where A is a large cation, B a smaller one, X is the anion and the r are the ionic radii of Shannon and Prewitt [33, 34], which depend on the coordination number and bonding specimens. The tolerance factors, t_G, of CsGeBr$_3$ and CsGeCl$_3$ crystal structure are 1.009(4) and 1.027, respectively (see the far right column in table 1). They are close to the empirically ideal perovskite structure with $t_G = 1.0$. However, these values slightly deviate from the ideal value of perovskite structure, 1.0, and could be the reason for the structural distortion.

2.5. Thermogravimetric measurements

Thermogravimetry (TG, %) and derivative thermogravimetry (DTG, mg min^{-1}) were employed to characterize the thermal and structural behaviours of CGB. Thermogravimetric analysis was carried out, on polycrystalline CsGeBr$_3$, in air at a heating rate of 5 °C min^{-1} to 550 °C with a Seiko 320 TG/DTA (thermogravimetry/differential thermal analysis). There were four parts of thermal and structural responses, which were observed in this thermogravimetric measurement (see figure 4). No significant weight loss or phase change was observed from room temperature up to 200 °C. Slight DTG peak of CGB at 242.9 °C indicated the phase change from rhombohedral to cubic. The phase change temperature was similar to
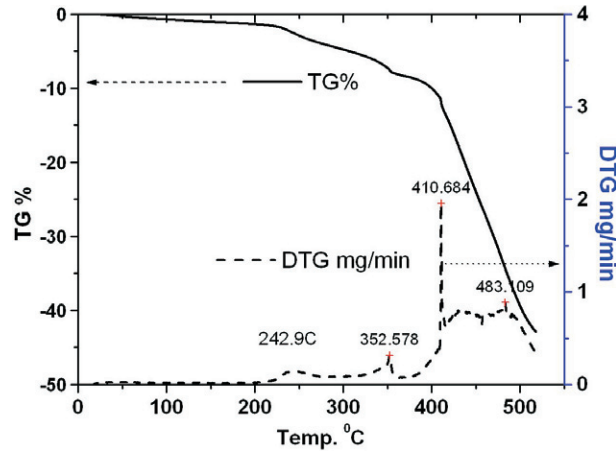
Figure 4. The thermal analysis of rhombohedral nonlinear optical crystal CsGeBr$_3$.

the reports of Thiele *et al* [16, 17]. The CsGeBr$_3$ became the liquid phase around 352.5 °C from cubic solid state phase when the temperature increased. The temperature DTG peak at 410.7 °C showed that CGB was thermally decomposed when the temperature was higher 410.7 °C. In summary, the NLO CsGeBr$_3$ crystal could be properly operated under 200 °C.

3. Nonlinear optical properties

The *ab initio* calculation of optical properties, e.g. dielectric function, and nonlinear coefficients of rhombohedral nonlinear optical crystals, CsGeX$_3$ (X = Cl, Br and I), were performed. The nonlinear coefficients of rhombohedral nonlinear optical crystals, CsGeX$_3$ (X = Cl and Br), will be presented and compared with the PSHG measurement.

3.1. Ab initio calculation on second-order nonlinear susceptibilities

For the second-order nonlinear optical (NLO) response, the theoretical description by Raskheev *et al* [35] was very complex. However, at the zero-frequency limits, the NLO susceptibility could be expressed as [36, 37]

$$\chi_{ijk}^{(2)}(0) = \frac{1}{V}\left(\frac{e\hbar}{m}\right)^3 \sum_k \sum_{vc}\Bigg[\sum_{c'}\frac{1}{E_{c'c}E_{cv}^2E_{c'v}^2}(D_{vc'c}^{ijk} + D_{cvc'}^{ijk} + D_{c'cv}^{ijk})$$
$$- \sum_{v'}\frac{1}{E_{vv'}E_{cv}^2E_{c'v}^2}(D_{v'cv}^{ijk} + D_{vv'c}^{ijk} + D_{cvv'}^{ijk})\Bigg] \tag{4}$$

where $D_{nml}^{ijk} = \mathrm{Im}[p_{nm}^i(p_{ml}^j p_{ln}^k + p_{ml}^k p_{ln}^j)]/2$. Here $p_{cv}^i(k, \text{Å}^{-1})$ denoted the momentum matrix element (MME) from the conduction band c to the valence band v at the k-point of the BZ. For the photon energy $\hbar\omega$ of PSHG measurement well below the bandgap, 2.32 eV, frequency-dependent $\chi_{ijk}^{(2)}(-2\omega; \omega, \omega)$ and $n(\omega)$ were nearly constants in this frequency region [12, 38]. The static $\chi_{ijk}^{(2)}(0)$ could be considered as a good approximation to the frequency-dependent $\chi_{ijk}^{(2)}(-2\omega; \omega, \omega)$ in the PSHG measurements.

Tang *et al* used the same approach by using both the local-density approximation (LDA) and the generalized-gradient approximation (GGA) with norm-conserving pseudopotentials to
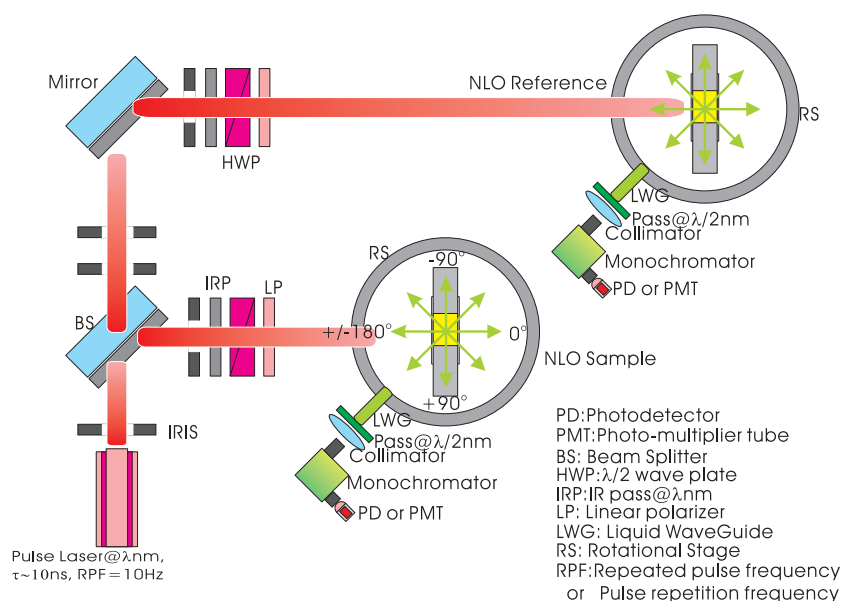
Figure 5. Experimental set-up used for measuring the second-harmonic scattering pattern from a crystalline powder sample.

investigate the electronic structures, optical and bulk properties of the rhombohedral ternary halides [10] and the orthorhombic ternary nitrides [36]. The analysis with band-by-band and atomic species projection techniques [10, 36] both yielded useful information about material properties and provided deep insight into the fundamental understanding of the electronic structures and optical properties of rhombohedral nonlinear optical crystals, CsGeX$_3$ (X = Cl, Br and I). A kinetic-energy cut-off of 580 eV, four special k points and 54 bands were used to ensure the convergence in the calculation of the optical properties.

Various representative calculations of nonlinear bulk susceptibilities which adopt the summations-over-excited-states (SOS) scheme were discussed in the review paper of Champagne and Bishop [25]. The models and calculating schemes employed in *ab initio* calculations progressed in parallel to the development of *ab initio* band structure calculation. The scissors operator approximation, one of the bandgap correction schemes, was good enough. In this study, we focused on the structural and the constituent effect on the NLO susceptibilities. There will be no bandgap correction scheme implemented, discussed or developed. In section 3.3 the calculated and the experimental results will be compared and discussed.

3.2. Second-order nonlinear optical measurements

Powder SHG measurements, which were reported by Chen *et al* [38], were performed on a modified Kurtz-NLO [39] system using 1064 nm light (figure 5).

A Q-switched Nd–YAG laser, operating at 10 Hz, was used for all measurements. The average energy and the pulse width per pulse were 3 mJ and 10 ns, respectively. Since the SHG efficiency of powders has been shown to depend strongly on particle size [39, 40], polycrystalline CsGeBr$_3$ was ground and sieved (Newark Wire Cloth Company) into six distinct particle-size ranges, 37 μm, 37–74 μm, 74–105 μm, 105–210 μm, 210–420 μm

and 420–840 μm. To make relevant comparison with known SHG materials, crystalline KDP was also ground and sieved into the same particle-size ranges. All of the powders were placed in separate capillary tubes. The SHG, i.e. 532 nm green light, radiation was collected in reflection and detected by a photomultiplier tube (Oriel Instruments). To detect only the SHG light, a 532 nm narrow-band-pass interference filter was attached to the tube. The SHG signal was collected by a data-acquisition (DAQ) interface and was monitored by a personal computer with the analysis program.

If the SHG process was phase-matchable and satisfied the type-I phase matching condition, the intensity of SHG response could be written as [41]

$$I_{2\omega}(\bar{r}, \theta) = \frac{128\pi^5 I_\omega^2}{n_\omega^2 n_{2\omega} \lambda_{2\omega}^2 c} L\bar{r}\langle d_{\text{eff}}^2 \rangle \frac{\sin^2[\frac{\pi}{2}\frac{\bar{r}}{l_{\text{pm}}}(\theta - \theta_{\text{pm}})]}{[\frac{\pi}{2}\frac{\bar{r}}{l_{\text{pm}}}(\theta - \theta_{\text{pm}})]} \tag{5}$$

where $\bar{l}_{\text{pm}} = \lambda/[4|\Delta n_{B,2\omega}| \sin 2\theta_{\text{pm}}]$, and θ_{pm} is the phase-matching angle. Here $\Delta n_{B,2\omega} = n_{E,2\omega} - n_{O,2\omega}$ denoted the birefringence of material at the second-harmonic wavelength. In the event that $\bar{r} \gg \bar{l}_{\text{pm}}$ or $\bar{r} \ll \bar{l}_{\text{pm}}$, equation (5) could be simplified to

$$I_{2\omega} \to \begin{cases} [(256\pi^4 I_\omega^2)/(n_\omega^2 n_{2\omega} \lambda_{2\omega}^2 c)]L\bar{l}_{\text{pm}}\langle d_{\text{eff}}^2 \rangle, \longleftarrow \bar{r} \gg \bar{l}_{\text{pm}} \\ [(128\pi^5 I_\omega^2)/(n_\omega^2 n_{2\omega} \lambda_{2\omega}^2 c)]L\bar{r}\langle d_{\text{eff}}^2 \rangle, \longleftarrow \bar{r} \ll \bar{l}_{\text{pm}} \end{cases}. \tag{6}$$

The SHG signals became saturated when the average particle sizes were larger than $\bar{l}_{\text{pm}}$ and independent of the particle sizes.

Chen *et al* [38] derived a useful empirical formula, which possessed the correct asymptotic forms in equation (6), to depict the overall variation in second-harmonic intensity with particle size $\bar{r}$

$$I_{2\omega} = \frac{256\pi^4 I_\omega^2}{n_\omega^2 n_{2\omega} \lambda_{2\omega}^2 c} L\bar{l}_{\text{pm}}\langle d_{\text{eff}}^2 \rangle \sqrt{1 - \exp[-(\bar{r}/A)^2]} \tag{7}$$

with $A \approx 9\bar{l}_{\text{pm}}$.

An experimental arrangement for measuring the second-harmonic scattering pattern from crystalline powders is described in figure 5. In this set-up, the fundamental beam normally impinges on the sample cell. A liquid light guide with its input end attached on a rotation stage is employed to collect the second-harmonic intensity at various scattering angles. The second-harmonic pattern over scattering angle to yield the total second-harmonic intensity, $I_{2\omega}$, was integrated. The square of the effective nonlinearity, $\langle d_{\text{eff}}^2 \rangle$, averaged over the orientation distribution of crystalline powders of CsGeBr$_3$, was determined by equation (8) with a reference NLO crystal, e.g. KDP.

$$\langle d_{\text{eff}}^2 \rangle_{\text{CGB}} = \langle d_{\text{eff}}^2 \rangle_{\text{KDP}} \frac{I_{2\omega,\text{CGB}}^{\text{total}} n_{\omega,\text{CGB}}^2 n_{2\omega,\text{CGB}}}{I_{2\omega,\text{KDP}}^{\text{total}} n_{\omega,\text{KDP}}^2 n_{2\omega,\text{KDP}}} \approx \langle d_{\text{eff}}^2 \rangle_{\text{KDP}} \frac{I_{2\omega,\text{CGB}}^{\text{total}} n_{\text{CGB}}^3}{I_{2\omega,\text{KDP}}^{\text{total}} n_{\text{KDP}}^3} \tag{8}$$

when $n \approx n_\omega \approx n_{2\omega}$.

3.3. Nonlinear optical properties

Powder SHG measurements on sieved polycrystalline CGBr (figure 6) and CGC revealed that the SHG efficiencies of CGBr and CGC were higher than that of KDP. In figure 6, the detected SHG signals of CGBr in the higher (reflected) angle were saturated. The PMT detection sensitivity was kept at the same magnitude and was not lowered, because the SHG signals of KDP (reference) cannot be detected or identified in lower sensitivities. The integrated intensities were estimated from the reflection signals in various particle sizes, and showed the SHG responses of sieved polycrystalline CsGeBr$_3$ were about 1.62 times larger than that of
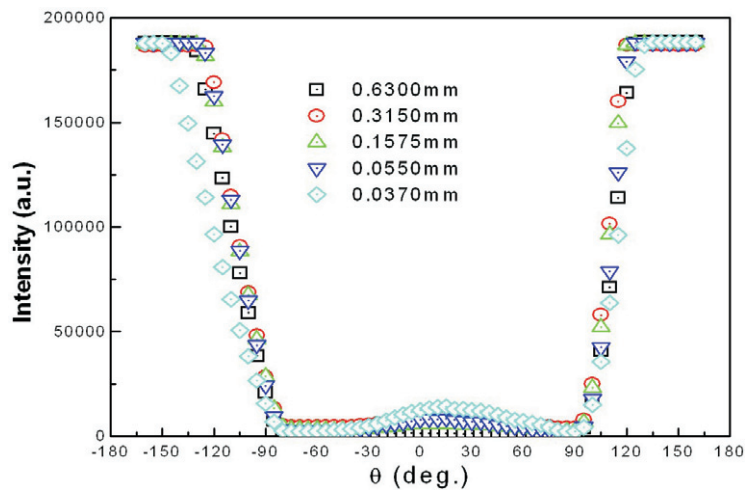
Figure 6. The powder second-harmonic generation results of rhombohedral nonlinear optical crystal CsGeBr$_3$.
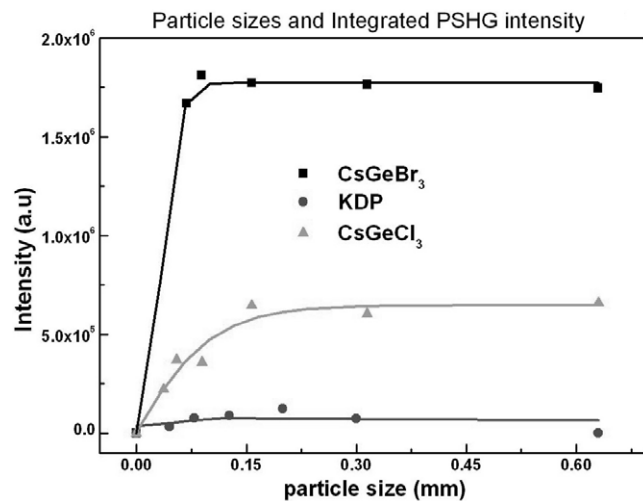
Figure 7. The comparison of integrated powder second-harmonic generation intensity of nonlinear optical crystal KDP, CsGeCl$_3$ and CsGeBr$_3$.

CsGeCl$_3$ and 9.63 times larger than that of KH$_2$PO$_4$ (KDP) (see table 2). In addition, both CsGeBr$_3$ and CsGeCl$_3$ were phase-matchable (see figure 7), as was KDP. That is, as the particle size becomes substantially larger than the coherence length of the crystal, the collected SHG intensity does not gain any more and saturates at a certain value. The estimate of the coherence length of the three crystals compared in this section is based on the position (particle size) of the saturation point. According to the relation between integrated $I_{2\omega}$ with respect to average particle size (figure 7), the coherence length L_c is $\approx 200\ \mu$m for KDP, $\approx 150\ \mu$m for CGC and $\approx 75\ \mu$m for CGB.

The CsGeBr$_3$ crystal is found in crystal class $3m$, which has the nonvanishing tensor elements $xzx = yzy, xxz = yyz, zxx = zyy, zzz, yyy = -yxx = -xxy = -xyx$ [3, 12, 13]

Table 2. Non-linear optical coefficients of NLO crystals CsGeBr$_3$, CsGeCl$_3$, KDP (as a reference) and BBO. They were integrated from the reflection powder second-harmonic generation signals in the same measured conditions.

| NLO crystal	n ($\lambda = 1.064 \ \mu$m)	d_{eff} (pm V^{-1})	$d_{\text{eff}}/d_{\text{KDP}}$
CsGeBr$_3$	2.31	3.46	9.63
CsGeCl$_3$	2.30	2.12	5.90
KDP	1.50	0.36	1.00
BBO	1.66	1.66	4.61

Table 3. Second-order non-linear optical susceptibilities of rhombohedral CsGeCl$_3$, CsGeBr$_3$ and CsGeI$_3$ crystals. They were estimated from the *ab initio* correction scheme without employing the bandgap.

NLO crystal	$\chi_{zzz}^{(2)}$ (pm V^{-1})	$\chi_{xyy}^{(2)}$ (pm V^{-1})
CsGeCl$_3$	3.698	0.925
CsGeBr$_3$	10.40	1.112
CsGeI$_3$	28.36	0.918

assuming Kleinman symmetry is valid [42]. For comparison, *ab initio* calculated second-order non-linear optical susceptibilities of rhombohedral CsGeCl$_3$, CsGeBr$_3$ and CsGeI$_3$ crystals are shown in table 3. They were estimated from the *ab initio* calculation without integrating the bandgap correction scheme.

The d_{eff}, which was measured by PSHG method, was the accumulated effect, and the PSHG method served as a screening technique of choosing proper NLO materials. It is hard to simulate the second-order NLO tensors, $d_{ijk}^{(2)}$ or $\chi_{ijk}^{(2)}$, from a powder measurement. However, the response trends of $d_{\text{eff}}^{(2)}$, $d_{ijk}^{(2)}$ and $\chi_{ijk}^{(2)}$ should be similar. Besides, there is a semi-empirical rule: $d_{\text{eff}}^{(2)} \approx d_{ijk}^{(2)} = 1/2\chi_{ijk}^{(2)}$ [12]. In general, the magnitude of $\chi_{ijk}^{(2)}$ is about double that of $d_{\text{eff}}^{(2)}$. The calculated second-harmonic generation signal of CGB was $\approx$2.8 times larger than that of CGC crystal and $\approx$2.7 times smaller than that of CGI crystal. The major susceptibilities were increased as the atomic weight of halides was increased. This tendency is similar to the previous PSHG measurement. The measured NLO susceptibility of CGBr was not as large as the calculated one. The detected signals of CGBr in the high reflection angles (see figure 6) were saturated, because the signals were much stronger than the detection threshold on PMT. If the detection threshold on PMT were rearranged to lower sensitivity to fulfil the stronger signal requirement, the signals of CGC and KDP would be too weak to detect or identify (figure 7). The reflected SHG signals and the under-estimated $d_{\text{eff}}^{(2)}$ of CGB could be rescaled to $\approx$5.19 by a factor $\approx$1.50. The rescaled $d_{\text{eff}}^{(2)}$ of CGBr was about 2.45 times larger than that of CsGeCl$_3$, and was about half of the calculated $\chi_{ijk}^{(2)}$.

There are some reasons for the significant SHG signals of rhombohedral CsGeBr$_3$ crystal. First of all, the SHG responses were contributed from the structural distortion and the off-centred Ge ion in the unit cell. The cell angle distortion of CGB is larger than that of CGC. The position of B-site cation, Ge, is closer to the cell corner than that of CGC. The $\chi_{zzz}^{(2)}$ increases as these distortions increase. Second, the bandgap values decreased [14–18, 10] and the NLO susceptibilities increased when the atomic weights of halides increased. The $\chi_{ijk}^{(2)}$ is approximately inversely proportional to the cube of the bandgap value [25, 12, 43] (see equation (4)). A third contribution has also been suggested, that the electron lone pair, the unbonding electron pair, of Ge, which was polarized in the [111] direction, could give more
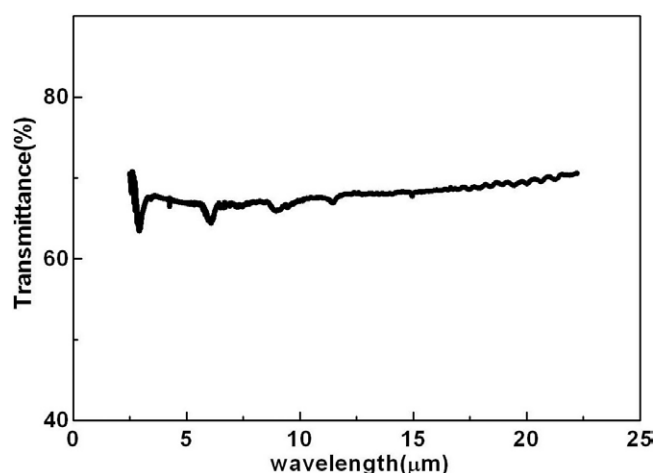
Figure 8. The transmission analysis of rhombohedral nonlinear optical crystal CsGeBr$_3$ in the mid-infrared range.

contribution to the MME summation. The lone-pair polarization was also mentioned in the reports by Thiele *et al* [14–18]. These reasons could form important guidelines for further NLO crystal designation.

4. Infrared measurements

Infrared spectra were recorded on the (*Perkin Elmer Instruments Spectrum One*) spectrometer in the range from 400 to 4000 cm^{-1}, i.e. 2.5–25 μm, with the sample pressed between two KBr pellets.

The transmittance of CsGeBr$_3$ powder was higher than 60% in the mid-infrared range, from 2.5 to 22.5 μm (see figure 8). That meant SHG signals could transmit in an NLO CsGeBr$_3$ single crystal. This transmission property in the IR spectrum was similar to other NLO ternary halides, e.g. CsGeCl$_3$, CsGeI$_3$ and superior to NLO oxide crystals, e.g. BBO and KTP.

5. Conclusions

According to the powder x-ray diffraction pattern and powder SHG results, an innovative infrared nonlinear optical crystal CsGeBr$_3$, which was characterized as a rhombohedral crystal structure, was synthesized. *Ab initio* calculations on CsGeBr$_3$ were also carried out to analyse the related electronic and optical properties. The space group symmetry of rhombohedral CsGeBr$_3$ was found to be *R*3*m* (No 160) and had no inversion centre. The reflection powder second-harmonic generation measurement of CGBr also showed that its nonlinear optical efficiency was larger than that of rhombohedral CsGeCl$_3$ by about 1.62 times and KDP by about 9.63 times. Saturated PSHG integration results of increasing powder particle sizes revealed that rhombohedral CsGeBr$_3$ was phase-matchable. The infrared transparent spectrum of rhombohedral CsGeBr$_3$ was extended to more than 22.5 μm. The rhombohedral CsGeBr$_3$ can be applied to infrared region as a potential nonlinear optical element.

Acknowledgments

References

[1] Burland D M 1994 *Chem. Rev.* **94** 1
[2] Chemla D S and Zyss J (ed) 1987 *Nonlinear Optical Properties of Organic Molecules and Crystals* (Orlando, FL: Academic)
[3] Dmitriev V G, Gurzadyan G G and Nikogosyan D N 1999 *Handbook of Nonlinear Optical Crystals* 3rd edn (Berlin: Springer)
[4] Zhang J, Su N, Yang C, Qin J, Ye N, Wu B and Chen C 1998 *Proc. SPIE* **3556** 1
[5] Zhang J 1995 *PhD Thesis* Wuhan University, Department of Material Science
[6] Ewbank M D, Cunningham F, Borwick R, Rosker M J and Gunter P 1997 *CLEO'97 Paper* vol CFA7, p 462
[7] Gu Q, Pan Q, Wu X, Shi W and Fang C 2000 *J. Cryst. Growth* **212** 605–7
[8] Gu Q, Pan Q, Shi W, Sun X and Fang C 2000 *Prog. Cryst. Growth Charact. Mater.* **40** 89–95
[9] Gu Q, Fang C, Shi W, Wu X and Pan Q 2001 *J. Cryst. Growth* **225** 501–4
[10] Tang L-C, Chang C-S and Huang J Y 2000 *J. Phys.: Condens. Matter* **12** 9129
[11] Ren P, Qin J and Chen C 2003 *Inorg. Chem.* **42** 8–10
[12] Boyd R W 2003 *Nonlinear Optics* 2nd edn (Boston, MA: Academic)
[13] Nye J F 1957 *Physical Properties of Crystals* (Oxford: Oxford University Press)
[14] Schwarz U, Hillebrecht H, Kaupp M, Syassen K, von Schnering H-G and Thiele G 1995 *J. Solid State Chem.* **118** 20–7
[15] Schwarz U, Wagner F, Syassen K and Hillebrecht H 1996 *Phys. Rev.* B **53** 12545
[16] Thiele G, Rotter H W and Schmidt K D 1987 *Z. Anorg. Allg. Chem.* **545** 148
[17] Thiele G, Rotter H W and Schmidt K D 1988 *Z. Anorg. Allg. Chem.* **559** 7–16
[18] Seo D-K, Gupta N, Whangbo M-H, Hillebrecht H and Thiele G 1998 *Inorg. Chem.* **37** 407
[19] Christensen A N and Rasmussen S E 1965 *Acta Chem. Scand.* **19** 421
[20] Tananaev I V, Dzhurinskii D F and Mikhailov Y N 1964 *Zh. Neorg. Khim.* **9** 1570–7
[21] Kraus W and Nolze G 1996 *J. Appl. Crystallogr.* **29** 301–3
[22] Payne M C, Teter M P, Allan D C, Arieas T A and Joannopoulos J D 1992 *Rev. Mod. Phys.* **64** 1045
[23] Segall M D, Lindan P L D, Probert M J, Pickard C J, Hasnip P J, Clark S J and Payne M C 2002 *J. Phys.: Condens. Matter* **14** 2717
[24] Monkhorst H J and Pack J D 1976 *Phys. Rev.* B **13** 5188
[25] Champagne B and Bishop D M 2003 *Adv. Chem. Phys.* **126** 41
[26] Goldschmidt V M 1927 *Ber. Dtsch. Chem. Ges.* **60** 1263
[27] Goldschmidt V M 1931 *Fortschr. Min.* **15** 73
[28] Galasso F S 1990 *Perovskites and High T Superconductors* (New York: Gordon and Breach)
[29] Butler V, Catlow C R, Fender B E F and Harding J H 1982 *Solid State Ion.* **8** 109–13
[30] Tejuca L G, Fierro J L G and Tascon J M D 1989 *Adv. Catal.* **36** 237–328
[31] Yokokawa H, Sakai N, Kawada T and Dokiya M 1992 *Solid State Ion.* **52** 43–56
[32] Thomas N W 1997 *Br. Ceram. Trans.* **96** 7–15
[33] Shannon R D and Prewitt C T 1969 *Acta Crystallogr.* B **25** 925
[34] Shannon R D 1976 *Acta Crystallogr.* A **32** 751–67
[35] Rashkeev S N, Lambrecht W R L and Segall B 1998 *Phys. Rev.* B **57** 3905
[36] Huang J Y, Tang L C and Lee M H 2001 *J. Phys.: Condens. Matter* **13** 10417
[37] Tang L C, Lee M H, Yang C H, Huang J Y and Chang C S 2003 *J. Phys.: Condens. Matter* **15** 6043
[38] Chen W K, Cheng C M, Huang J Y, Hsieh W F and Tseng T Y 2000 *J. Phys. Chem. Solids* **61** 969–77
[39] Kurtz S K and Perry T T 1968 *J. Appl. Phys.* **39** 3798–813
[40] Dougherty J P and Kurtz S K 1976 *J. Appl. Crystallogr.* **9** 145–58
[41] Prasad P N and Williams D J 1991 *Introduction to Nonlinear Optical Effects in Molecules and Polymers* (New York: Wiley) chapter 6
[42] Kleinman D A 1962 *Phys. Rev.* **126** 1977–9
[43] Shen Y R 2002 *The Principles of Nonlinear Optics* (New York: Wiley)